

## Supporting Information:

### Layer Hybridized Exciton-Plasmon Resonances for Enhanced Dispersion Modes in CuS:Al Nanostructured Films

Harkawal Singh<sup>1</sup>, Sandeep Kumar<sup>1</sup>, Thakur Sudesh Kumar Raunija<sup>2</sup> and Praveen Kumar Sharma<sup>1,3\*</sup>

<sup>1</sup>Department of Physics, DAV University, Sarmastpur, Jalandhar 144012, Punjab, India

<sup>2</sup>VFD Quality Control Division, Semi-Conductor Laboratory, Sector 72, SAS Nagar, Mohali-160071, India

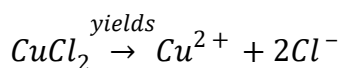
<sup>3</sup>Department of Nano Science and Materials, Central University of Jammu, Rahya Suchani (Bagla), Samba-181143, UT of J & K, India

\*Corresponding Author: Mob: +91-9501825252; E-mail: prafiziks@gmail.com

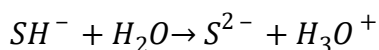
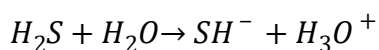
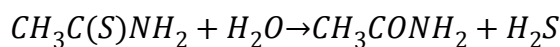
#### SI-1) Reaction mechanism

The synthesized CuS:Al system is comprised of multiple type of chemicals via ionic reactants ( $\text{Cu}^+$ ,  $\text{Cu}^{2+}$ ,  $\text{Al}^{3+}$ ,  $\text{S}^{2-}$ ) and complexing agents (Triton X-100, acetic acid and HCL). Here, all the cation/anion salts would initially undergo through complicated metastable states of ion-ligand bonds that finally resulted to affect oxide defect states and copper/ sulfur vacancies to synthesize the desired nanostructures as observed. Therefore, the generalized reaction mechanism is given according to the available type of precursor.

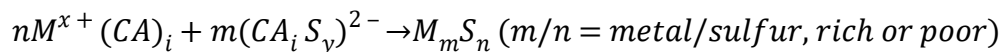
Here, the copper is available in both +1 and +2 ionic states from two different ionic precursors that on dissociation provide Cu ion as [S1]:



Whereas, the pH dependent hydrolysis of thioacetamide (TA) yields hydrogen sulfide ( $\text{H}_2\text{S}$ ) and acetamide ( $\text{CH}_3\text{CONH}_2$ ) that can be further dissociated to the sulfur ions:



The released ions from both sources made complexes with available yield complexing agents  $(CA)_i$  in solution to yield final CuS:Al nanostructures, which has been generalized as [S2, S3]:



where  $M^{x+} = Cu^+, Cu^{2+}$  and  $Al^{3+}$ .

### SI-2) FE-SEM (cross-sectional) and XRD (without baseline correction) micrographs

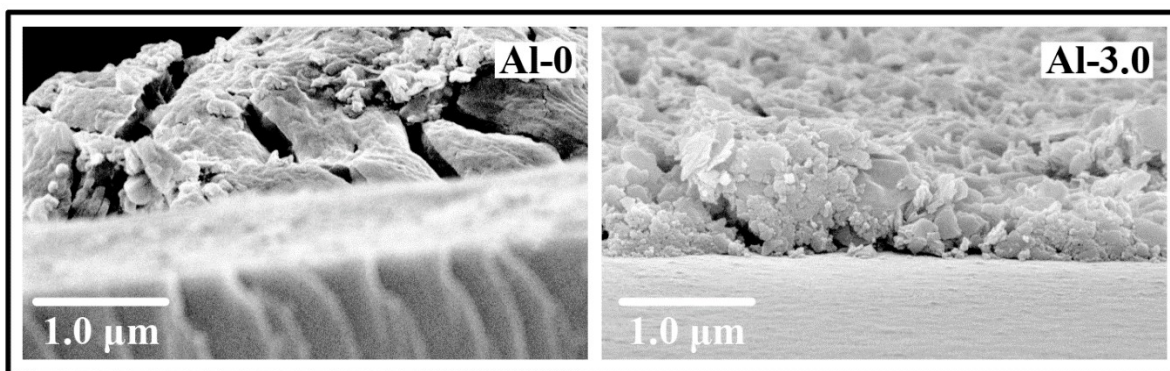


**Figure S1.** The cross-sectional view of CuS:Al nanostructured films.

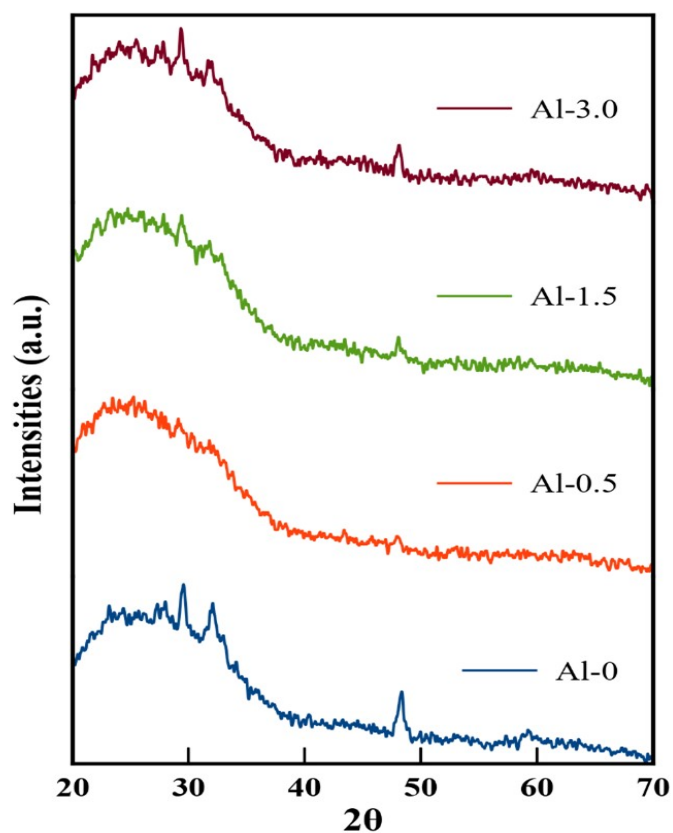


**Figure S2.** X-ray diffraction pattern without baseline correction for pristine and Al:CuS nanostructures

### SI-3) Kramers-Kronig constrained Drude-Lorentz relations to fit reflectance spectrum

The strong coupling between hybrid states has been treated as oscillator strength which is directly evidenced in the anti-crossing dispersion of the angle-resolved reflectance spectroscopy. However, the equally robust and straight-forward technique is the use of polarization-resolved reflectance spectra measured by Fourier-transform infrared spectrometry or UV-Vis-NIR spectrometer in near normal incidence mode. Here, the polarization free the complex reflection coefficient ( $r$ ) of air-film interface at normal incidence also become phase independent and get simplified as [S4, S5]:

$$r = \sqrt{R} \exp(i\theta) = \frac{1 - \sqrt{\epsilon}}{1 + \sqrt{\epsilon}}$$

where, ( $R$ ) is reflectance and ( $\epsilon$ ) is complex permittivity. The reflectance valley typically develops near the screened plasma frequency  $\omega_p^* = \omega_p / \sqrt{\epsilon_\infty}$ , where  $\epsilon_\infty$  is the permittivity at high frequency. Quantitative analysis of the plasma frequency can be used to fit the multiple resonances in reflectance curves according to the complex dielectric function of Drude-Lorentz oscillator model. This damped harmonic oscillator determines the wave energy transfer to atomic oscillations from light matter coupling and can be described as:

$$\epsilon(\omega) = \epsilon_\infty - \sum_{j=1}^n \frac{\omega_{p,j}^2}{\omega^2 + i\omega\tau_j} + \sum_k \frac{\Omega_{p,k}^2}{\omega_{0,k}^2 - \omega^2 - i\omega\gamma_k}$$

where, ( $j$  &  $k$ ) are the total number of higher-energy oscillators with the corresponding resonant frequency  $\omega_{0,k}$ ,  $\omega_{p,j}$  are the free carrier plasma frequencies for electrons and holes,  $\tau_j$  are the free carrier scattering times for electrons and holes,  $\Omega_{p,k}$  are the oscillator strengths for phonons and interband electronic transitions,  $\omega_{0,k}$  are the phonon and interband transition frequencies, and  $\gamma_k$  is the width of the corresponding transition. The parameter  $\epsilon_\infty$  is the contribution from the higher-frequency oscillators. Further, the relationship between complex counterparts for these calculated coefficients is established by Kramers-Kronig relations as:

$$n(\omega) - 1 = \frac{2}{\pi} P \int_0^\infty \frac{\omega' \kappa(\omega')}{\omega'^2 - \omega^2} d\omega'$$

where, real part known as dispersion  $n(\omega)$ , the imaginary parts known as attenuation coefficient  $\kappa(\omega)$  and  $P$  denoted the Cauchy principal value of the integral. Conclusively, the varied valley wave numbers reflect anisotropy in the plasma frequency which can be used in above mathematical structure to procure information on complex optical functions.

#### SI-4) Results of oscillator model fitting on reflectance Spectra

**Table S1:** The best-fit optical parameters used to model sample Al-0 at each measured reflectance data points and in consistent with film thickness estimated from FE-SEM measurements. The values for  $\epsilon_\infty$  were made constrained to be consistent with other fitting values and  $\chi^2$  signifies goodness of collective fit of parameterization.

Al-0					
$\chi^2 = 2.38E-05$					
$\epsilon_\infty = 1.853825 \pm 0.000000$					
No. of Oscillator	1	2	3	4	5
	(Drude Oscillator)	Lorentzian Oscillators			
$\omega_0$ (Cm <sup>-1</sup> )	0.000000 ± 0.000000	6299.732248 ± 0.000000	9677.510524 ± 0.000000	18983.526929 ± 0.000000	33333.000000 ± 0.000000
$\omega_p$ (Cm <sup>-1</sup> )	19028.478569 ± 0.000000	7701.161728 ± 0.000000	9178.377705 ± 0.000000	12947.802822 ± 0.000000	29886.521474 ± 0.000000
Y (Cm <sup>-1</sup> )	1749.772732 ± 0.000000	4601.796396 ± 0.000000	6252.050818 ± 0.000000	9386.124958 ± 0.000000	25275.383517 ± 0.000000

**Table S2:** The best-fit optical parameters used to model sample Al-0.5 at each measured reflectance data points and in consistent with film thickness estimated from FE-SEM measurements. The values for  $\epsilon_\infty$  were made constrained to be consistent with other fitting values and  $\chi^2$  signifies goodness of collective fit of parameterization.

Al-0.5				
$\chi^2 = 1.23E-06$				
$\epsilon_\infty = 1.95 \pm 0.000000$				
No. of Oscillator	1	2	3	4
	(Drude Oscillator)	Lorentzian Oscillators		
$\omega_0$	0.000000 ± 0.000000	9174.263132 ± 0.000000	17565.760314 ± 0.000000	33193.674352 ± 0.000000
$\omega_p$	18870.383004 ± 0.000000	14787.260892 ± 0.000000	11419.872073 ± 0.000000	23247.073983 ± 0.000000
Y	4104.580619 ± 0.000000	12470.698091 ± 0.000000	7545.402469 ± 0.000000	23974.201016 ± 0.000000

**Table S3:** The best-fit optical parameters used to model sample Al-1.5 at each measured reflectance data points and in consistent with film thickness estimated from FE-SEM measurements. The values for  $\epsilon_\infty$  were made constrained to be consistent with other fitting values and  $\chi^2$  signifies goodness of collective fit of parameterization.

<b>Al-1.5</b>				
$\chi^2 = 1.39E-06$				
$\epsilon_\infty = 1.95 \pm 0.000000$				
<b>No. of Oscillator</b>	<b>1</b>	<b>2</b>	<b>3</b>	<b>4</b>
	<b>(Drude Oscillator)</b>	<b>Lorentzian Oscillators</b>		
$\omega_0$	0.000000 $\pm$ 0.000000	8685.854911 $\pm$ 0.000000	18094.963391 $\pm$ 0.000000	33481.384265 $\pm$ 0.000000
$\omega_p$	15197.667868 $\pm$ 0.000000	12951.132064 $\pm$ 0.000000	9146.277331 $\pm$ 0.000000	24229.298504 $\pm$ 0.000000
$\Upsilon$	4039.044228 $\pm$ 0.000000	11378.777273 $\pm$ 0.000000	5455.896642 $\pm$ 0.000000	23024.716441 $\pm$ 0.000000

**Table S4:** The best-fit optical parameters used to model sample Al-3.0 at each measured reflectance data points and in consistent with film thickness estimated from FE-SEM measurements. The values for  $\epsilon_\infty$  were made constrained to be consistent with other fitting values and  $\chi^2$  signifies goodness of collective fit of parameterization.

<b>Al-3.0</b>				
$\chi^2 = 1.40E-06$				
$\epsilon_\infty = 2.056498 \pm 0.000000$				
<b>No. of Oscillator</b>	<b>Drude Oscillator 1</b>	<b>Lorentzian Oscillators</b>		
		<b>2</b>	<b>3</b>	<b>4</b>
$\omega_0$	0.000000 $\pm$ 0.000000	9909.000633 $\pm$ 0.000000	17689.895474 $\pm$ 0.000000	32364.544927 $\pm$ 0.000000
$\omega_p$	22404.777127 $\pm$ $\pm 0.000000$	1833.147634 $\pm$ 0.000000	14035.249232 $\pm$ 0.000000	27446.472047 $\pm$ 0.000000
$\Upsilon$	8953.213810 $\pm$ 0.000000	1958.910322 $\pm$ 0.000000	7462.426305 $\pm$ 0.000000	28159.239173 $\pm$ 0.000000

### SI-5) The calculated other optical parameters

Surface plasmon frequency ( $\omega_{sp}$ ) is associated with screened plasmon frequency and with linewidth of that resonance band as described in equation below [S6]:

$$\omega_{lsp} = \sqrt{\frac{\omega_p^2}{\epsilon_\infty + 2\epsilon_m} - \gamma^2}$$

where all the symbols have standard meaning. In the case of nano-films surrounding medium is air-film interface for which the medium dependent factor ( $2\epsilon_m \sim 1$ ).

Quality factor of surface plasmons reflects the information on the strength of their field. This factor specifically depends upon the geometry and environment of nanoparticles [S4, S5]. Nanoparticles in colloidal form are considered to be in quasi static regime which have high optical resolution behaviour, so can be directly estimated from the linear ratio of dielectric constants as:  $Q_{sp} = -\epsilon_r/\epsilon_i$ . Whereas, in case of thin films, nanoparticles stacked up to form nanostructures where dispersive behaviour dominates results in non-uniform distribution of quality factor throughout regime, hence, gained its dependence on complex refractive index as:  $Q_{sp} = k/2n$  [S6, S7].

### SI-6) Linear Absorption Spectroscopy:

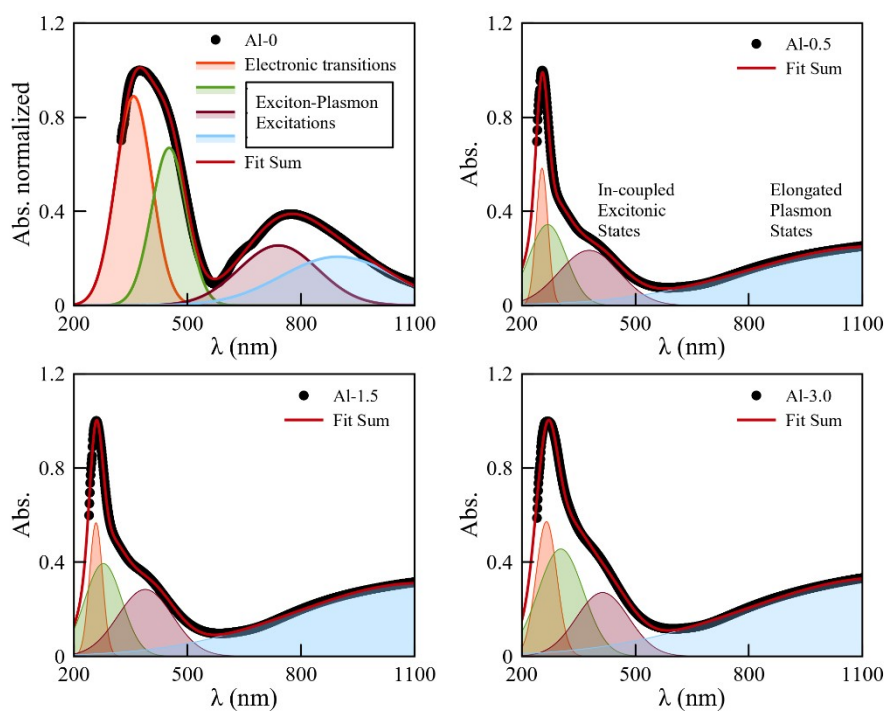


**Figure S3.** The resolved characteristic of coupled exciton-plasmon resonances in linear absorption spectra.

It can be observed that with the addition of  $\text{Al}^{3+}$  ion from Al-0.5 to Al-3.0, the coupling regime has shifted from plasmon dominated domain to inter-exciton interactive region along with broadened NIR plasmon energy states. It can be due to the presence of plasmon-excitation of Al element in UV-Vis region that enhances  $1S_h-1S_e$  excitonic transitions to arise two photon absorption mechanism that results in the shift of energy band or coupling mechanism [S8]. The increasing incorporation of  $\text{Al}^{3+}$  doping is also exhibit in the increasing FWHM of these optically resolved hybrid states. Therefore, it can be concluded that the  $\text{Al}^{3+}$  incorporation have enhanced in-couplings of excitonic states that can tune sub-wavelength modes for better volume of concentrated light interactions.

### SI-7) XPS Spectroscopy

The survey scan of CuS nanostructured films signalling peaks for Cu, S along with standard recognised peaks for C and O at 285.0 eV and 532.0 eV respectively. Narrow scan spectra of each concerned constituent have been extracted for precise calculations of charge oxidation states of different elements. Here, the relative atomic % ratio of all present element species have been element species have been evaluated from the area of all significant peaks in XPS survey scan. Simultaneously, the total relative change in ratio of Al-content with respect to Cu vacancies for  $\sim 76$  eV B.E. is also evaluated.

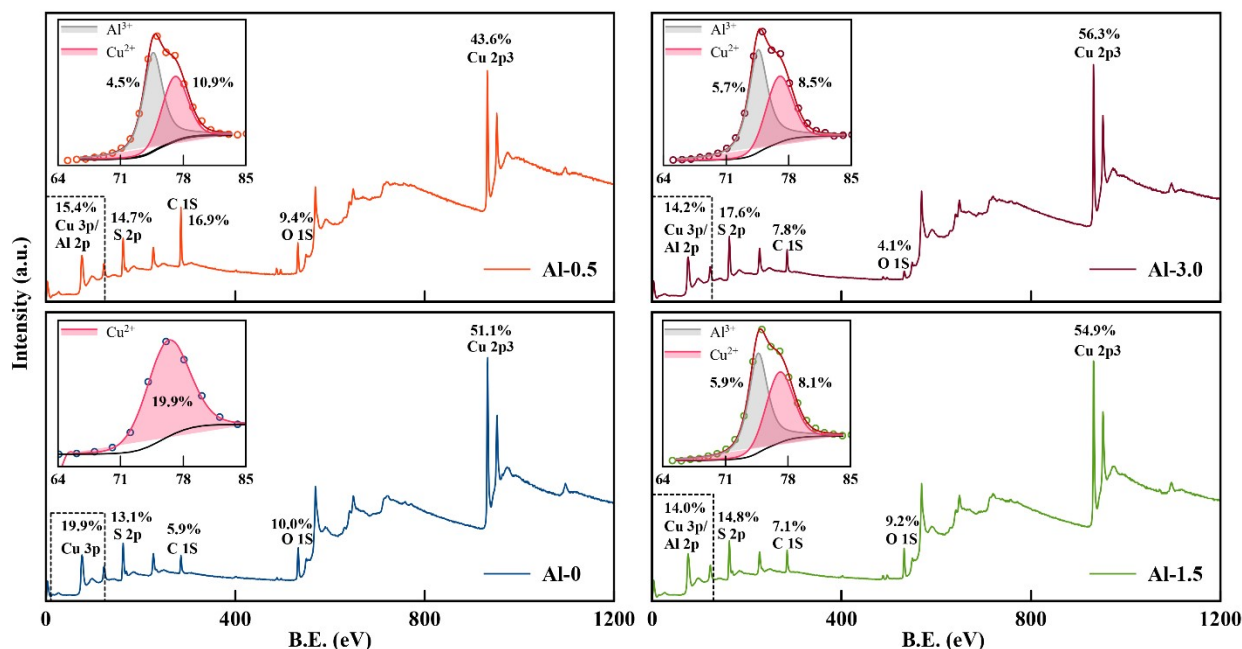


**Figure S4.** XPS survey scan with estimated relative atomic % of present elements in CuS:Al nanostructured films. (subset) The relative distribution of Al-O w.r.t Cu vacancies corresponding to Al-doping concentration.

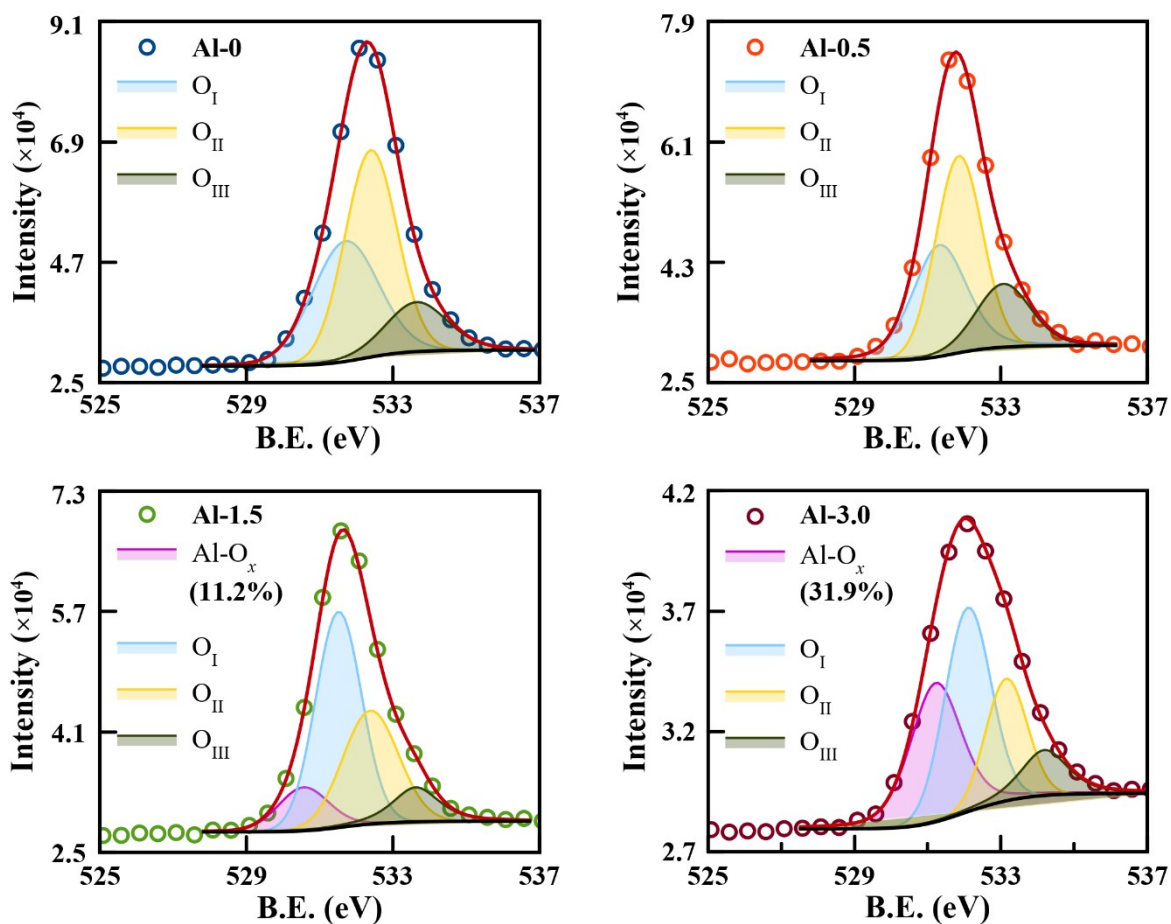


**Figure S5.** The deconvoluted O1s spectra for the traces of oxygen species ( $O_2^-$ ,  $O^{2-}$  or  $O^-$ ) and Al-dopant concentration.

The binding energies of the O 1s peaks were divided into three peaks lying between 531.7 - 533.9 eV. These O-components of higher binding energy is usually attributed to chemisorbed and dissociated oxygen species ( $O_2^-$ ,  $O^{2-}$  or  $O^-$ ) and OH [S9]. For convenience, these are marked as O<sub>I</sub>, O<sub>II</sub>, and O<sub>III</sub> for O 1s peak. The oxygen species with a lower binding energy of 530.3 eV are attributed to AlO<sub>x</sub> (OH) component [S9]. At low Al-doping in Al-0.5, the significant peaks of oxygen species shifted to lower binding energy without any physical trace of Al-O<sub>x</sub> states. However, in sample Al-1.5 and Al-3.0, the relative proportions of Al-O<sub>x</sub> states are started to appear and their relative atomic % increases with increase in doping concentration.

## References

- S1. A.D. Savariraj, H.J. Kim, K.K. Viswanathan, M.V. Kumar and K. Prabakar, *RSC Adv.*, 2016, **6**, 19034.
- S2. A.A. Shults, G. Lu, J.D. Caldwell and J.E. Macdonald, *Nanoscale Horiz.*, 2023, Advance Article, DOI: <https://doi.org/10.1039/D3NH00227F>

- S3. S. A. McLuckey and T. Y. Huang, *Anal. Chem.*, 2009, **81**, 8669.
- S4. K. Zhang, Y. Du, Z. Qi, B. Cheng, X. Fan, L. Wei, L. Li, D. Wang, G. Yu, S. Hu, C. Sun, Z. Huang, J. Chu, X. Wan and C. Zeng, *Phys. Rev. Appl.*, 2020, **13**, 014058.
- S5. A.B. Kuzmenko, *Rev. Sci. Instrum.*, 2005, **76**, 1–9.
- S6. J. Luther, P. Jain, T. Ewers and A.P. Alivisatos, *Nature Mater.*, 2011, **10**, 361–366.
- S7. M.G. Blaber, M.D. Arnold and M.J. Ford, *J. Condens. Matter Phys.*, 2010, **22**, 15.
- S8. E. Cao, W. Lin, M. Sun, W. Liang and Y. Song, *Nanophotonics*, 2018, **7**, 145–167.
- S9. A. Liu, G. Liu, H. Zhu, B. Shin, E. Fortunato, R. Martins and F. Shan, *RSC Adv.* 2015, **5**, 86606.